© 2019. Published by The Company of Biologists Ltd | Journal of Cell Science (2019) 132, jcs228916. doi:10.1242/jcs.228916

SHORT REPORT

Colocation of Tpm3.1 and myosin IIa heads defines a discrete subdomain in stress fibres

Joyce C. M. Meiring[1,‡], Nicole S. Bryce[1,‡], Maria Lastra Cagigas[1,‡], Aleš Benda[2,*], Renee M. Whan[2], Nicholas Ariotti[1,3], Robert G. Parton[4,5], Jeffrey H. Stear[1], Edna C. Hardeman[1] and Peter W. Gunning[1,§]

ABSTRACT

Co-polymers of tropomyosin and actin make up a major fraction of the actin cytoskeleton. Tropomyosin isoforms determine the function of an actin filament by selectively enhancing or inhibiting the association of other actin binding proteins, altering the stability of an actin filament and regulating myosin activity in an isoform-specific manner. Previous work has implicated specific roles for at least five different tropomyosin isoforms in stress fibres, as depletion of any of these five isoforms results in a loss of stress fibres. Despite this, most models of stress fibres continue to exclude tropomyosins. In this study, we investigate tropomyosin organisation in stress fibres by using super-resolution light microscopy and electron microscopy with genetically tagged, endogenous tropomyosin. We show that tropomyosin isoforms are organised in subdomains within the overall domain of stress fibres. The isoforms Tpm3.1 and 3.2 (hereafter Tpm3.1/3.2, encoded by *TPM3*) colocalise with non-muscle myosin IIa and IIb heads, and are in register, but do not overlap, with non-muscle myosin IIa and IIb tails. Furthermore, perturbation of Tpm3.1/3.2 results in decreased myosin IIa in stress fibres, which is consistent with a role for Tpm3.1 in maintaining myosin IIa localisation in stress fibres.

KEY WORDS: Tropomyosin, Myosin II, APEX, Actin filament organisation

INTRODUCTION

Stress fibres are typically contractile structures that allow cells to respond to mechanical force, to remodel connective tissue and apply force to their external environment (Pellegrin and Mellor, 2007; Tojkander et al., 2012; Burridge and Wittchen, 2013). Contractile stress fibres are made up of bundles of actin filaments, crosslinked by α-actinin and non-muscle myosin IIa and/or IIb (isoforms of myosin II with the heavy chain encoded by *MYH9* and *MYH10*, respectively), organised in a repetitive, sarcomere-like fashion (Hu et al., 2017; Tojkander et al., 2012). Tropomyosins form co-polymers with actin and determine the function of an actin filament in an isoform-dependent manner by altering its stability, affinity for other actin-binding proteins, and activity/engagement of myosins (Gunning et al., 2015). Various tropomyosin isoforms have been observed to localise to stress fibres, and the loss of individual tropomyosin isoforms compromises the entire structure (Tojkander et al., 2011). Given that the majority of actin filaments in cultured cells associate with tropomyosin, it is important to investigate the detailed organisation of tropomyosins in actin structures (Meiring et al., 2018).

High molecular weight (HMW) tropomyosin isoforms of Tpm1.6, 1.7 and 2.1 (encoded by *TPM1* and *TPM2*; hereafter, Tpm1.6/1.7/2.1), are not conducive to myosin II activity *in vitro* (Gateva et al., 2017); however, they are critical to stress fibre stability (Tojkander et al., 2011; Prasad et al., 1993). However, studies have suggested that tropomyosin isoforms Tpm3.1 and 3.2 (two nearly identical isoforms encoded by *TPM3* that are not distinguishable via antibody staining; hereafter denoted Tpm3.1/3.2) and Tpm4.2 (encoded by *TPM4*) recruit (Bryce et al., 2003; Tojkander et al., 2011) and support the activity of non-muscle myosin II *in vitro* (Gateva et al., 2017; Pathan-Chhatbar et al., 2018; Hundt et al., 2016), therefore these isoforms were predicted to colocalise with non-muscle myosin II striations.

U2OS cells were chosen for this study because stress fibres have been well characterised in these cells (Tojkander et al., 2011; Hotulainen and Lappalainen, 2006). U2OS cells contain three different types of stress fibres: dorsal, ventral and transverse arcs (Hotulainen and Lappalainen, 2006). Dorsal stress fibres are not contractile and serve to anchor transverse arcs to focal adhesions. Transverse arcs are contractile and fuse with dorsal stress fibres in order to produce ventral stress fibres (Hotulainen and Lappalainen, 2006). Ventral stress fibres are typically generated from several transverse arcs, reducing the likelihood that the sarcomere-like structures within them will be aligned. Transverse arcs show the best alignment of the sarcomere-like structures, therefore making this class of stress fibre optimal for examining molecular organisation. Since different tropomyosin isoforms impart different properties on actin filaments, these results imply that stress fibres are the product of actin filaments with different functions. However, confocal imaging has not been able to discern detailed localisation of tropomyosin isoforms within the context of the semi-sarcomeric structures in stress fibres (Schevzov et al., 2011; Tojkander et al., 2011).

Here, we use a super-resolution microscopy approach to dissect the organisation of tropomyosin isoforms in stress fibres. We show that Tpm isoforms have discrete periodic localisations along actin filaments and that Tpm3.1/3.2 colocalises with myosin II heads, but not with either myosin II tails or α-actinin. To confirm the periodic localisation, we generated a Tpm3.1/3.2–APEX2 mouse via CRISPR to identify Tpm3.1/3.2 on actin filaments using electron microscopy. By tagging endogenous Tpm3.1/3.2 with APEX2 *in vivo*, we show for the first time, the periodic localisation of an

[1]School of Medical Sciences, University of New South Wales, Sydney, NSW 2052, Australia. [2]Biomedical Imaging Facility, Mark Wainwright Analytical Centre, University of New South Wales, Sydney, NSW 2052, Australia. [3]Electron Microscope Unit, Mark Wainwright Analytical Centre, University of New South Wales, Sydney, NSW 2052, Australia. [4]Cell Biology and Molecular Medicine Division, Institute for Molecular Bioscience, University of Queensland, St Lucia, QLD 4072, Australia. [5]Centre for Microscopy and Microanalysis, University of Queensland, St Lucia, QLD 4072, Australia.

*Present address: Imaging methods core facility at BIOCEV, Faculty of Sciences, Charles University, Czech Republic.

‡These authors contributed equally to this work

§Author for correspondence (p.gunning@unsw.edu.au)

J.C.M.M., 0000-0001-9166-5363; N.S.B., 0000-0001-9799-7393; M.L.C., 0000-0001-5464-2349; R.M.W., 0000-0002-6664-6344; R.G.P., 0000-0002-7494-5248; E.C.H., 0000-0003-1649-7712; P.W.G., 0000-0003-0833-3128

Received 13 December 2018; Accepted 6 July 2019

Journal of Cell Science (2019) 132, jcs228916. doi:10.1242/jcs.228916

endogenous tagged tropomyosin on actin filaments using electron microscopy and tomography. These results allow us to postulate a new model for the organisation of a stress fibre. The model predicts that Tpm3.1/3.2 influences the association of myosin II with an actin filament. We test this relationship by removing Tpm3.1/3.2 from actin filaments using the compound ATM3507. This results in reduced association of myosin IIa with stress fibres.

RESULTS AND DISCUSSION

Tropomyosin isoforms localise in different regions along stress fibres

The anti-tropomyosin antibodies rabbit δ/9d (against Tpm4.1 and 4.2; hereafter, Tpm4.1/4.2) was paired with either mouse monoclonal CG3 (against Tpm3.1/3.2) or Tm311 (against Tpm1.6/1.7/2.1), to investigate the overlapping localisation of different tropomyosins within stress fibres. Two-colour STED microscopy of transverse arcs demonstrated that the subgroups of tropomyosin isoforms exhibited little overlap and appeared to be organised in segregated micro domains (Fig. 1A,B). From the STED images, discrete staining patterns are also evident for the different isoforms; a punctate pattern for Tpm4.1/4.2, a striated pattern for Tpm3.1/3.2 and largely continuous staining for the HMW tropomyosins Tpm1.6/1.7/2.1 (Fig. 1A,B). Line-scan analysis confirms these differences in organisation (Fig. 1A,B). These different staining patterns are in line with hypothesised functions for the different isoforms in stress fibres, and highlight the possibility that these different isoforms play spatially distinct roles in modulating stress fibre function. This result also favours the proposal that actin filaments are coated homogenously by either a single tropomyosin isoform or a subgroup of tropomyosin isoforms in cells (Bryce et al., 2003; Gunning et al., 2015; Gateva et al., 2017).

Tpm3.1/3.2 colocalises with non-muscle myosin II heads but not tails in stress fibres

We predicted that if Tpm3.1/3.2 was regulating myosin II activity, then myosin II heads, but not tails would localise specifically with Tpm3.1/3.2. To test this, we compared the localisation of Tpm3.1/3.2 with non-muscle myosin IIa and IIb, the two myosin forms enriched in stress fibres. By using STED microscopy and antibodies that recognise the non-helical tailpiece of myosin IIa and IIb, we found that Tpm3.1/3.2 was in register with the tail domain of both

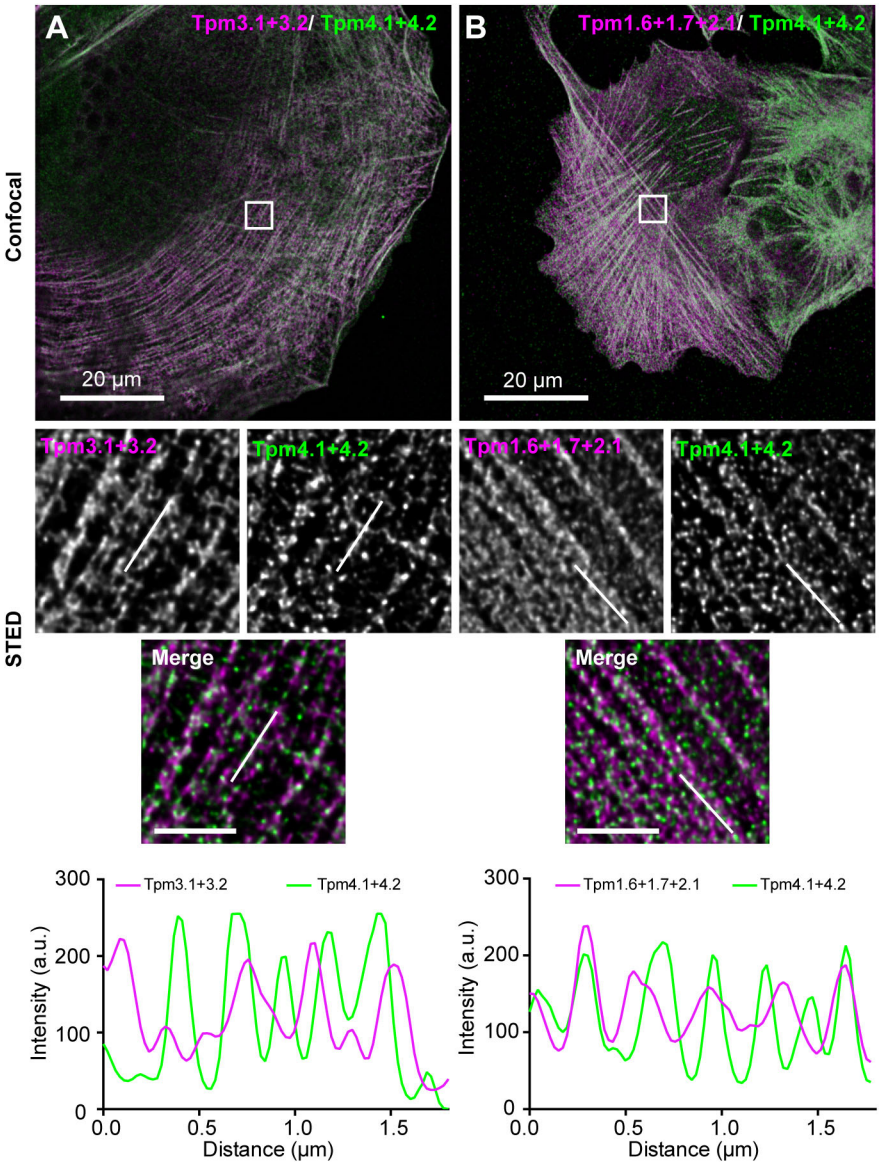

Fig. 1. Tropomyosins are organised in micro-domains within stress fibres. Representative confocal and two-colour STED images of U2OS cells fixed and immunostained for (A) Tpm3.1/3.2 (magenta) and Tpm4.1/4.2 (green) or (B) Tpm1.6/1.7/2.1 (magenta) and Tpm4.1/4.2 (green). One representative line-scan taken along a stress fibre (line indicated on all images) is displayed below. Scale bars: 20 µm (main images); 2 µm (magnifications).

myosin isoforms, but showed little overlap using line-scan analysis (Fig. 2A,B; Fig. S1A). This finding was consistent with our hypothesis, since the tail domain of myosin II does not interact with actin filaments, and hence would not be predicted to colocalise with Tpm3.1/3.2. Since there were no isoform-specific antibodies available that targeted the myosin II head region, we transfected cells with mEmerald–myosin IIa and mEmerald–myosin IIb which are N-terminally tagged, fluorescent non-muscle myosin II constructs that specifically label the head domain (Burnette et al., 2014). Since the mEmerald tag was incompatible with STED, we instead used Zeiss Airyscan semi-super-resolution imaging. Airyscan, while having a lower resolution than STED, has sufficiently high resolution to capture the myosin II head doublets in myosin II filaments (arrows, Fig. 2C,D). Tpm3.1/3.2 staining colocalised with both myosin IIa and IIb heads (Fig. 2C,D; Fig. S1A), as shown by line-scan analysis and supported by measurement of Manders' coefficient of the Airyscan images (Fig. S1C,D). In order to confirm that the colocalisation of Tpm3.1 with myosin IIa and IIb heads was not a staining artefact, we also investigated the localisation of fluorescently labelled Tpm3.1 construct Ruby2–N-Tpm3.1, with respect to mEmerald–myosin IIa in live cells. Ruby2–N-Tpm3.1 is observed to colocalise with mEmerald–myosin IIa (arrows, Fig. S1B), consistent with our immunofluorescence data.

To gain further context for the localisation of Tpm3.1 in stress fibres relative to other stress fibre components, we also tested its localisation relative to the actin-bundling protein α-actinin, another major component of stress fibres. STED microscopy of co-immunostained samples revealed that Tpm3.1/3.2 did not overlap with α-actinin in transverse arcs (Fig. 2E). This was consistent with previous findings showing that tropomyosins are not compatible with α-actinin in *in vitro* actin-binding assays (Gateva et al., 2017).

The striated organisation of Tpm3.1/3.2 was confirmed in stress fibres by performing transmission electron microscopy (TEM). We produced an endogenously APEX2-tagged Tpm3.1 (Tpm3.1–APEX2) mouse (Fig. 3A), from which we harvested mouse embryonic fibroblasts (MEFs) that also produce actin stress fibres with distinct myosin IIa striations (Fig. 3B). Tpm3.1–APEX2 imaged via electron microscopy in heterozygous MEFs showed enrichment in bands across actin bundles (white arrowheads, Fig. 3C–E). Actin filaments that did not contain any Tpm3.1–APEX2 were also identified (black arrowheads, Fig. 3C). The average distance between the striations was 328 nm±123 nm (n=5 actin bundles) (Fig. 3F). Tomograms of actin bundles in homozygous MEFs (Movie 1) confirmed the presence of Tpm3.1–APEX2 striations and also the existence of intact actin filaments in the sections (Fig. 3G, H; Movie 2). Both TEM and tomography confirm the striated organisation of Tpm3.1/3.2 observed with fluorescence microscopy. Together, our results indicate that Tpm3.1 localises to discrete regions in stress fibres, overlapping with myosin IIa and IIb heads.

The simplest model we can derive from our microscopy data is one where bundles of actin filaments cross-linked by α-actinin are associated with Tpm3.1/3.2 in the regions where myosin IIa/IIb heads associate with actin filaments (Fig. 3I). This model is also supported by previous work showing that Tpm3.1 overexpression enhances non-muscle myosin IIa recruitment to stress fibres (Bryce et al., 2003), and *in vitro* studies demonstrating the ability of Tpm3.1 to stabilise non-muscle myosin II on actin filaments and enhance its activity (Gateva et al., 2017; Pathan-Chhatbar et al., 2018; Hundt et al., 2016).

Disruption of Tpm3.1/3.2 via targeted drug treatment perturbs myosin IIa retention in stress fibres

Our colocalisation data and other previous studies (Bryce et al., 2003; Gateva et al., 2017) suggests that non-muscle myosin IIa and IIb associates with Tpm3.1/3.2-coated actin filaments. We therefore predicted that removal of Tpm3.1/3.2 from filaments may result in reduced non-muscle myosin II retention. While Tpm3.1/3.2 depletion disrupts the ability of cells to form stress fibres (Tojkander et al., 2011), recently characterised anti-Tpm3.1/3.2 drugs allow for more precise calibration of the magnitude of protein disruption. We therefore used an anti-Tpm3.1/3.2 drug, ATM3507 (Currier et al., 2017), at a concentration where Tpm3.1/3.2 localisation is disrupted without completely disassembling stress fibres, in order to assess the contribution of Tpm3.1/3.2 to myosin II colocalisation with stress fibres. The localisation of myosin IIa with stress fibres was diminished in drug-treated cells, although like Tpm3.1/3.2, some protein still colocalised with actin filaments (Fig. 4A). In contrast, the association of Tpm4.2, an isoform that is not impacted by ATM3507, with stress fibres was not disrupted with drug treatment (Fig. 4B). This is consistent with previous *in vitro* work indicating that Tpm3.1 enhances the activity of myosin II as well as its colocalisation with stress fibres (Pathan-Chhatbar et al., 2018; Gateva et al., 2017; Bryce et al., 2003). This is also consistent with the observation that Tpm3.1 recruitment to actin filaments precedes that of myosin II (Masedunskas et al., 2018).

In summary, we find that Tpm3.1/3.2 localise in discrete striations along stress fibres in both U2OS cells and MEFs. This is a clear demonstration that stress fibres do not consist of a homogeneous bundle of actin filaments but rather contain subdomains characterised by their tropomyosin isoform composition. We therefore suggest that stress fibres may be composed of different functional subdomains defined, at least in part, by their tropomyosin composition which provides an explanation of why stress fibres require five different tropomyosins for their assembly and/or maintenance (Tojkander et al., 2011). This is also in agreement with the recent demonstration that Tpm2.1- and Tpm1.6-containing actin filaments can be segregated within the same stress fibre in human foreskin fibroblasts and are engaged by myosin II motors to perform different functions (Sao et al., 2019).

The alignment of myosin IIa and IIb heads with Tpm3.1/3.2 has allowed us to construct a proposed organisation of a mini-contractile unit within stress fibres (Fig. 3I). The conservation of dimensions between the STED and electron microscopy in two cell types suggests that this may be a conserved structural unit.

MATERIALS AND METHODS

Cell culture

U2OS cells (human, female, derived from an osteosarcoma; ATCC) were cultured in DMEM (Sigma) supplemented with 10% fetal bovine serum (FBS; Gibco) at 37°C under 5% CO_2. Cells were confirmed to be mycoplasma free with tests performed using the PCR mycoplasma test kit (AppliChem GmbH) as per the manufacturer's instructions. mEmerald–myosin IIa (Burnette et al., 2014) and mEmerald–myosin IIb constructs were Addgene plasmid #54190 and #54192, respectively (deposited by Michael Davidson); mRuby2-N-Tpm3.1 was synthesised by GeneArt (Thermo Fisher Scientific). Plasmids were and transfected into cells using Lipofectamine 3000 (Thermo Fisher Scientific) according to manufacturer's instructions and cells were used for experiments 48 h post transfection.

Generation of Tpm3.1-APEX2 MEFs

Animal experiments were performed in accordance with UNSW Australia Animal Care and Ethics Committee approval and Australian National Health and Medical Research Council (NHMRC) guidelines. The mouse

Journal of Cell Science (2019) 132, jcs228916. doi:10.1242/jcs.228916

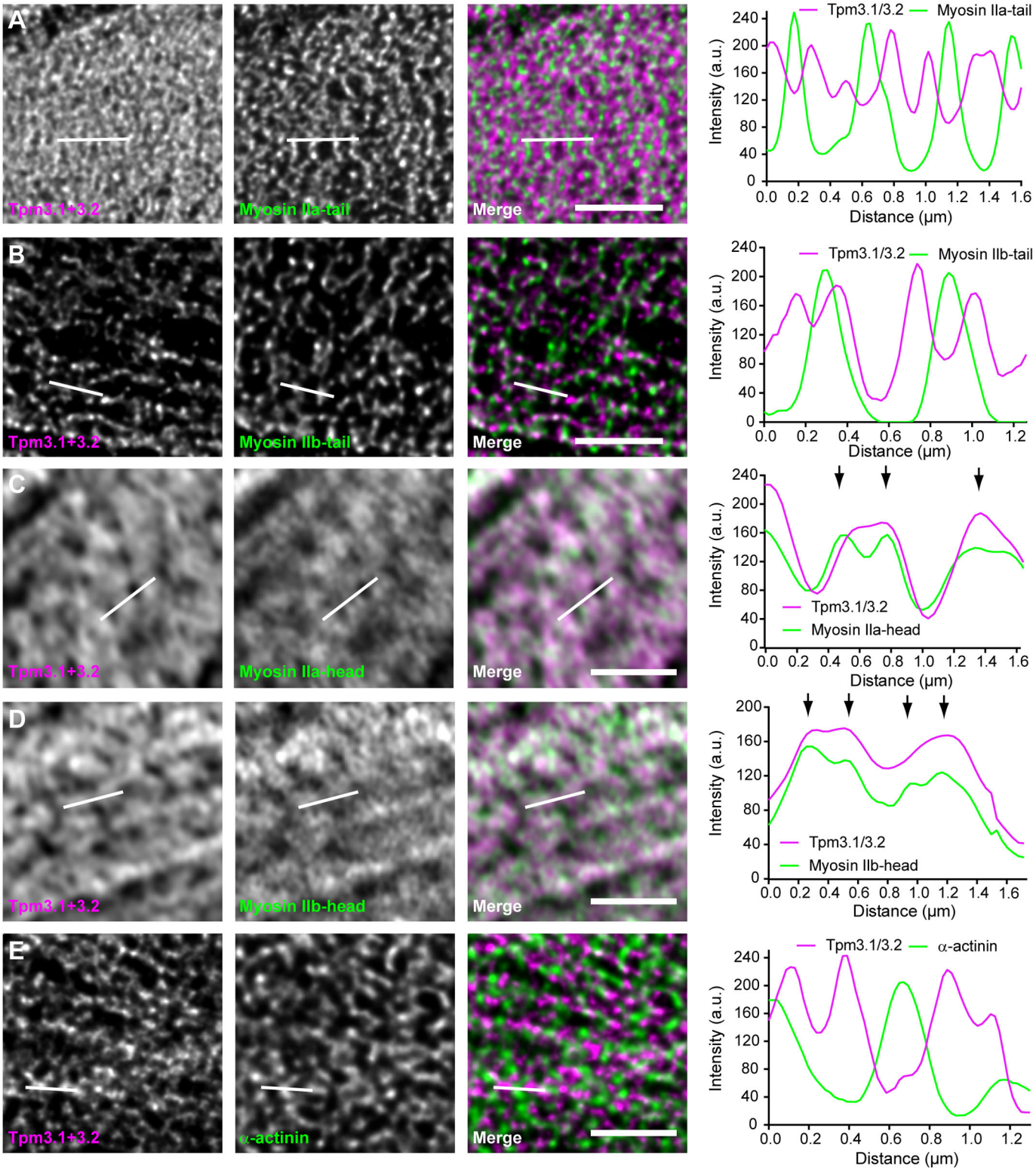

Fig. 2. Tpm3.1/3.2 overlaps with non-muscle myosin II heads but not with non-muscle myosin II tails or α-actinin in stress fibres. (A,B) STED images of transverse arcs in U2OS cells that were fixed and co-stained with antibodies against Tpm3.1/3.2 and the tail domain of non-muscle myosin IIa (A) or non-muscle myosin IIb (B). Per image, one representative line-scan taken along a stress fibre (line indicated on all images) is displayed on the right. (C,D) Airyscan confocal images of transverse arcs in U2OS cells transfected with either mEmerald–myosin IIa (C) or mEmerald–myosin IIb (D) to label the myosin heads, then fixed and stained with an antibody against Tpm3.1/3.2. Per image, one representative line-scan taken along a stress fibre (line indicated on images) is displayed on the right. Line-scans highlight the overlap of myosin II head peaks (arrows) with Tpm3.1/3.2. (E) STED images of transverse arcs in U2OS cells that were fixed and co-stained with antibodies against Tpm3.1/3.2 and α-actinin. One representative line-scan taken along a stress fibre (line indicated on images) is displayed on the right. Scale bars: 2 µm. Confocal images of the whole cells showing the regions where the STED and airyscan images were taken from are shown in Fig. S1.

Journal of Cell Science (2019) 132, jcs228916. doi:10.1242/jcs.228916

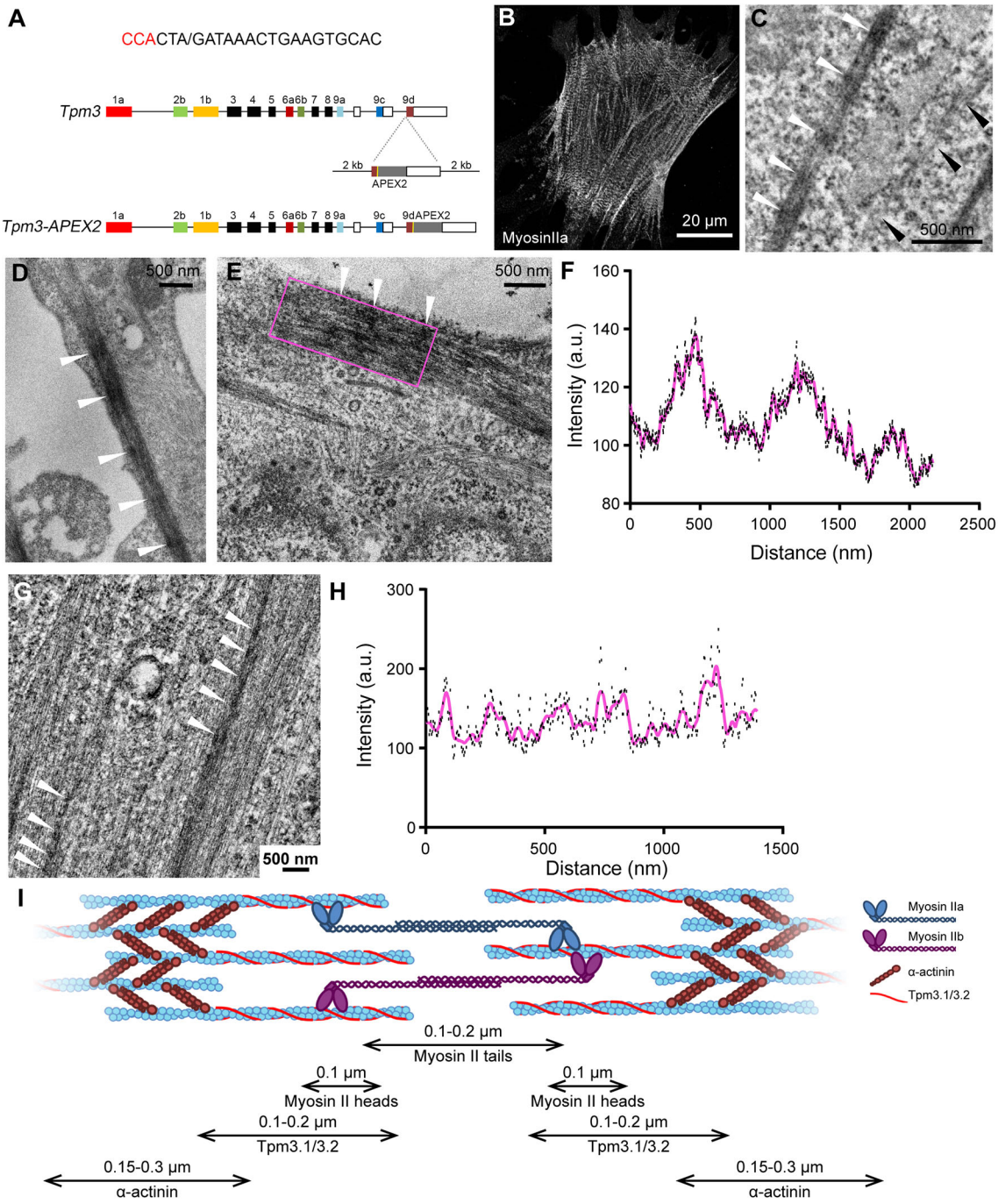

Fig. 3. Tpm3.1 is periodically localised along an actin filament. (A) A mouse line expressing Tpm3.1 C-terminally tagged with APEX2 from the endogenous locus was generated using CRISPR. One high-scoring guide RNA (gRNA) sequence was selected, '/' indicates the cut site, NGG, in red. The plasmid repair template consisted of 2 kb homology arms flanking a mutated PAM site (TCA), exon 9d, a 10-amino-acid linker, and the APEX2 sequence inserted in frame with exon 9d. (B) Maximum-intensity projection airyscan confocal image of Tpm3.1–APEX2 MEFs stained for myosin IIa showing that the Tpm3.1–APEX2 primary MEF cells also have distinct myosin striations. (C) TEM images of Tpm3.1–APEX2 construct in Tpm3.1–APEX2 +/– primary MEFs showing that Tpm3.1–APEX2 is organised in striations in cortical actin bundles. White arrowheads show Tpm3.1–APEX2 organised in distinct striations along the filament, and black arrowheads show an actin filament bundle that does not contain Tpm3.1–APEX2. (D,E) TEM images of Tpm3.1–APEX2 construct in Tpm3.1–APEX2 +/– primary MEFs showing that Tpm3.1–APEX2 is organised in striations in cortical actin bundles. (F) A histogram representing the line-scan of the actin bundle from the magenta rectangle in E. (G) An average intensity *z*-projection of a tomogram of Tpm3.1–APEX2 primary +/+ MEF cells with APEX2 densities highlighted with white arrowheads. (H) A histogram representing the line-scan of the 5-arrowhead-long actin bundle. Scale bars as indicated. (I) A proposed model of the organisation of Tpm3.1/3.2, myosin II and α-actinin in stress fibres based on STED, airyscan and TEM microscopy data.

line B6-*Tpm3*$^{tm6(APEX2)Hrd}$ which expresses Tpm3.1 C-terminally tagged with APEX2 from the endogenous locus was generated by Cyagen using CRISPR. The strategy of targeting this exon via CRISPR was similar to that previously published (Masedunskas et al., 2018), with the APEX2 sequence (Ariotti et al., 2017) instead of the mNeon Green sequence inserted in frame with exon 9d (Fig. 3A). C57Bl/6 mouse zygote pronuclei were injected with Cas9 mRNA, CRISPR guide RNA and circular plasmid donor. Surviving zygotes were transferred to pseudo-pregnant female recipients and the

Journal of Cell Science (2019) 132, jcs228916. doi:10.1242/jcs.228916

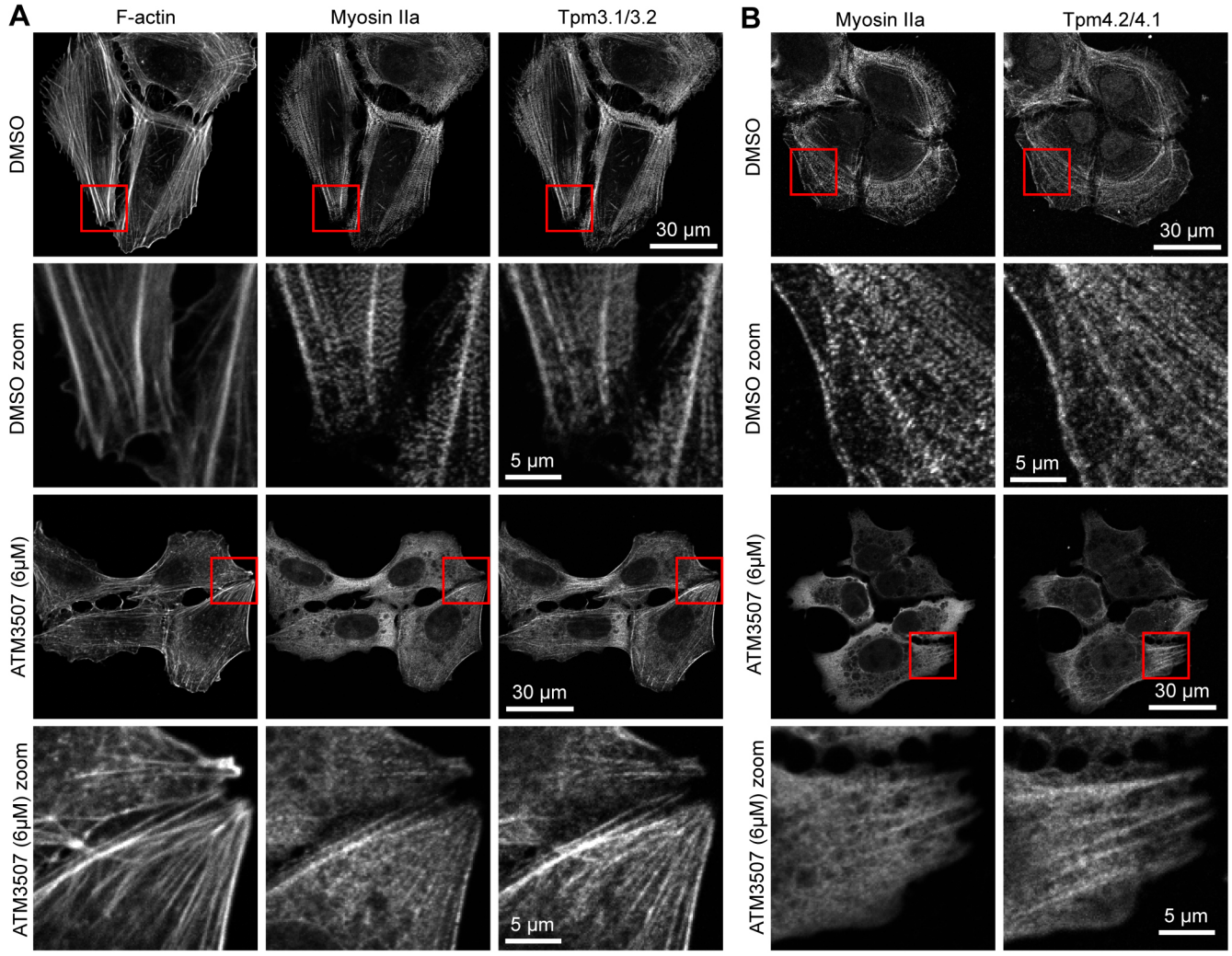

Fig. 4. The anti-Tpm3.1 drug ATM3507 perturbs non-muscle myosin IIa localisation. Single-plane confocal images of U2OS cells treated for 24 h with either DMSO or 6 µm ATM3507, and fixed and stained for (A) F-actin, non-muscle myosin IIa or Tpm3.1/3.2 or (B) myosin IIa and Tpm4.1/4.2. The area in the red box is enlarged and shown below the image it is taken from.

resulting pups screened for homologous integration of the donor template by PCR using genomic DNA. The animals were genotyped by PCR using forward primer 5′-TCTTTGTCCTTGTCTGGAGTGGTC-3′ and reverse primer 5′-CAGCACTCACAGTTGGGTAAGAC-3′ resulting in a 478 bp band for the knock-in allele. The knock-in was confirmed via sequencing. Primary MEFs were isolated from day 13.5 B6-*Tpm3*$^{tm6(APEX2)Hrd}$ mouse embryos and cultured as previously described (Schevzov et al., 2005).

Immunofluorescence

Cells grown on #1.5 glass coverslips were fixed for 30 min in warmed 1% paraformaldehyde in DMEM with 20 mM HEPES. Coverslips were subsequently washed with PBS and permeabilised with ice-cold methanol for 5 min. Methanol was carefully diluted out with PBS so as to prevent drying out or damaging samples, and coverslips were blocked in 5% BSA in PBS for 1 h. Primary antibodies were diluted in blocking buffer and incubated on coverslips for 1 h. Coverslips were washed three times with PBS and incubated with secondary antibodies in blocking buffer for another hour. Coverslips were washed with PBS three times and mounted with Mowiol (Sigma) mounting medium. The primary antibodies used were as follows: STAR635p-conjugated mouse anti-Tpm3.1,3.2 (CG3, 1:50, Schevzov et al., 2011), mouse anti-Tpm1.6,1.7,2.1 (Tm311, 1:200, Sigma-Aldrich; cat. no. #T2780), mouse anti-α-actinin (BM-75.2, 1:500, Sigma- Aldrich cat. no. A5044); sheep anti-Tpm3.1,3.2 (γ/9d, 1:100, Percival et al., 2004), rabbit anti-Tpm4.2 [δ/9d (2009), 1:50, Schevzov et al., 2011], mouse anti-myosin IIa (1:250, Abcam cat. no. ab55456), rabbit anti-myosin IIa (1:250, Abcam cat. no. ab24762), mouse anti-myosin IIb (1:200, Abcam cat. no. ab684), and rabbit anti-myosin IIb (1:250, Covance cat. no. PRB-445P) antibodies. The secondary antibodies used were as follows: STAR635p-conjugated goat anti-mouse-IgG (1:500, Abberior cat. no. 2-0002-007-5), STAR580-conjugated goat anti-mouse-IgG (1:500, Abberior cat. no. 2-0002-005-1); STAR635p-conjugated goat anti-rabbit-IgG (1:500, Abberior cat. no. 2-0012-007-2); STAR580-conjugated goat anti-rabbit-IgG (1:500, Abberior cat. no. 2-0012-005-8) and STAR635p-conjugated donkey anti-sheep-IgG (1:250) antibodies.

STED microscopy

STED images were acquired on a Leica TCS SP5 STED confocal microscope fitted with a 100×/1.4 oil STED objective and linked to a PicoQuant Microtime 200 with single-photon avalanche diode detectors and a PicoHarp 300 Time-Correlated Single Photon Counting System. 532 nm and 635 nm excitation pulsed Diode lasers were synchronised to a depletion multiphoton laser tuned to 750 nm. Data was acquired in Time Tagged Time-Resolved format using PH300 data acquisition software and images were extracted using a TTTR data analysis program, both written by and available from A.B., then deconvolved using Huygens Deconvolution software.

Airyscan microscopy

Airyscan confocal microscopy was performed on a Zeiss 880 equipped with a Plan-Apochromat 63×/1.4 NA Oil DIC M27 objective and an Airyscan

detector. Samples were illuminated using 488 nm, 561 nm or 633 nm lasers, and all data was collected and processed using the Zen software (Zeiss).

Sample preparation for electron microscopy

Tpm3.1-APEX2 +/− and +/+ primary MEFs were seeded onto MatTek 35 mm no. 1.5 gridded coverslips and grown to 70–80% confluency. All sample processing was performed according to manufacturer's instructions in a PELCO BioWave microwave fitted with a PELCO ColdSpot Pro System for temperature control and using a PELCO EM Pro Vacuum Chamber. Cells were fixed in 2.5% glutaraldehyde (Electron Microscopy Sciences, Hatfield, PA) in 0.1 M sodium cacodylate buffer (pH 7.4; Sigma-Aldrich). After fixation, cells were washed in 0.1 M sodium cacodylate buffer. To prepare the 3′3-diaminobenzidine tetrahydrochloride (DAB; Sigma-Aldrich) mixture, DAB was dissolved in H_2O and vortexed for 3 min. The solution was diluted to a final concentration of 1 mg DAB/ml and 0.1 M sodium cacodylate, vortexed and syringe-filtrated using a 0.2 µm filter (Millipore). Cells were washed with DAB at room temperature for 2 min followed by a 30 min DAB wash supplemented with 5.88 mM H_2O_2 (Sigma-Aldrich) to generate the reaction product. After DAB treatment, cells were washed in 0.1 M sodium cacodylate buffer and post-fixed with 1% osmium tetroxide (OsO_4) in 0.1 M sodium cacodylate buffer to create an electron dense product surrounding Tpm3.1. Cells were washed in 0.1 M sodium cacodylate buffer and in H_2O. Serial dehydration was performed with 30%, 50%, 70%, 90% and 2×100% ethanol in double distilled H_2O. Serial infiltration was performed with 33%, 66% and 2×100% LX112 resin (Ladd, Williston, VT) in ethanol. Cells were flat-embedded using a resin bullet and resin was polymerised at 60°C for 16–24 h. After 30 min cooling at room temperature, polymerised cell-containing bullets were snapped off and the glass coverslip was cooled in liquid nitrogen and gently removed. Cells were visualised using a dissecting microscope (Leica EZ4, Leica Microsystems) and the resin was trimmed around them. Ultrathin 70 nm horizontal sections were cut using a 45° diamond knife (Diatome) on an ultramicrotome (Leica EM UC6, Leica Microsystems) and gently placed on formvar-coated mesh grids (ProSciTech).

Electron microscopy

Grids were imaged on a Tecnai G2 20 TEM transmission electron microscope at 200 kV at 7000× magnification. Cells were imaged with a 2k×2k BM Eagle Camera at 7000 times magnification with a binning of 1. Tomograms were acquired as described previously (Ariotti et al., 2015). Briefly, thick (200 nm) sections were cut on a Leica UC6 ultramicrotome and were coated with 10 nm fiducial gold markers. Dual axis tilt series were collected on a 200 kV Talos Arctica (Thermo Fisher) operated at room temperature. Unbinned 4k×4k images were acquired in two directions with 2° increments encompassing −60° to +60° on a Falcon 3 camera (Thermo Fisher) operated in linear mode under the control of Tomography software (Thermo Fisher Scientific). Tilt series were reconstructed using weighted back-projection in IMOD (Ariotti et al., 2015). Segmentation of tropomyosin-decorated actin filaments was performed using the Isosurface Render program in IMOD.

Image analysis

Images were analysed in ImageJ. Line-scan analysis was performed by drawing region of interest lines across stress fibres or cortical actin bundles in the case of the Tpm3.1–APEX2 TEM data. Manders' co-occurrence analysis was performed using the JACoP plugin in ImageJ.

Acknowledgements

We would like to thank Tom Hall (IMB, University of Queensland) for advice on Apex sequences, the UNSW Biomedical Imaging Facility staff for technical assistance, and Pekka Lappalainen (University of Helsinki) for helpful discussions. The authors acknowledge the Victor Chang Innovation Centre, funded by the NSW Government, and the use of facilities at the Electron Microscope Unit and Biomedical Imaging Facility within the Mark Wainwright Analytical Centre at UNSW Sydney, funded in part by the NSW Government.

Competing interests

E.C.H. and P.W.G. are directors and shareholders in TroBio Therapeutics, a company that is commercialising anti-tropomyosin drugs for the treatment of cancer and their labs receive funding from TroBio to evaluate anti-tropomyosin drug candidates. J.C.M.M., N.S.B., M.L.C., A.B., R.M.W., N.A. and R.G.P. have no competing interests.

Author contributions

Conceptualization: J.C.M.M., P.W.G.; Methodology: J.C.M.M., N.S.B., M.L.C., A.B., R.M.W., N.A., J.H.S.; Software: A.B.; Validation: J.C.M.; Formal analysis: J.C.M., N.S.B., M.L.C., N.A., R.G.P.; Investigation: J.C.M.M., N.S.B., M.L.C., J.H.S.; Writing - original draft: J.C.M.M.; Writing - review & editing: J.C.M.M., N.S.B., M.L.C., A.B., R.M.W., N.A., R.G.P., J.H.S., E.C.H., P.W.G.; Visualization: J.C.M.M., N.S.B.; Supervision: N.S.B., R.M.W., R.G.P., E.C.H., P.W.G.; Project administration: N.S.B., E.C.H., P.W.G.; Funding acquisition: R.G.P., E.C.H., P.W.G.

Funding

This work was supported by the National Health and Medical Research Council of Australia [project grant numbers APP1100202, APP1079866, APP1140064 and APP569542]; Australian Research Council [grant number DP16010162 and Centre of Excellence in Convergent Bio-Nano Science and Technology]; R.G.P. holds a NHMRC Senior Principal Research Fellowship. P.W.G. and E.C.H. received support from the Kids Cancer Project.

Supplementary information

Supplementary information available online at
http://jcs.biologists.org/lookup/doi/10.1242/jcs.228916.supplemental

References

Ariotti, N., Rae, J., Leneva, N., Ferguson, C., Loo, D., Okano, S., Hill, M. M., Walser, P., Collins, B. M. and Parton, R. G. (2015). Molecular characterization of Caveolin-induced membrane curvature. *J. Biol. Chem.* **290**, 24875-24890. doi:10.1074/jbc.M115.644336

Ariotti, N., Hall, T. E. and Parton, R. G. (2017). Correlative light and electron microscopic detection of GFP-labeled proteins using modular APEX. *Methods Cell Biol.* **140**, 105-121. doi:10.1016/bs.mcb.2017.03.002

Bryce, N. S., Schevzov, G., Ferguson, V., Percival, J. M., Lin, J. J.-C., Matsumura, F., Bamburg, J. R., Jeffrey, P. L., Hardeman, E. C., Gunning, P. et al. (2003). Specification of actin filament function and molecular composition by tropomyosin isoforms. *Mol. Biol. Cell* **14**, 1002-1016. doi:10.1091/mbc.e02-04-0244

Burnette, D. T., Shao, L., Ott, C., Pasapera, A. M., Fischer, R. S., Baird, M. A., Der Loughian, C., Delanoe-Ayari, H., Paszek, M. J., Davidson, M. W. et al. (2014). A contractile and counterbalancing adhesion system controls the 3D shape of crawling cells. *J. Cell Biol.* **205**, 83-96. doi:10.1083/jcb.201311104

Burridge, K. and Wittchen, E. S. (2013). The tension mounts: stress fibers as force-generating mechanotransducers. *J. Cell Biol.* **200**, 9-19. doi:10.1083/jcb.201210090

Currier, M. A., Stehn, J. R., Swain, A., Chen, D., Hook, J., Eiffe, E., Heaton, A., Brown, D., Nartker, B. A., Eaves, D. W. et al. (2017). Identification of cancer-targeted tropomyosin inhibitors and their synergy with microtubule drugs. *Mol. Cancer Ther.* **16**, 1555-1565. doi:10.1158/1535-7163.MCT-16-0873

Gateva, G., Kremneva, E., Reindl, T., Kotila, T., Kogan, K., Gressin, L., Gunning, P. W., Manstein, D. J., Michelot, A. and Lappalainen, P. (2017). Tropomyosin isoforms specify functionally distinct actin filament populations in vitro. *Curr. Biol.* **27**, 705-713. doi:10.1016/j.cub.2017.01.018

Gunning, P. W., Hardeman, E. C., Lappalainen, P. and Mulvihill, D. P. (2015). Tropomyosin - master regulator of actin filament function in the cytoskeleton. *J. Cell Sci.* **128**, 2965-2974. doi:10.1242/jcs.172502

Hotulainen, P. and Lappalainen, P. (2006). Stress fibers are generated by two distinct actin assembly mechanisms in motile cells. *J. Cell Biol.* **173**, 383-394. doi:10.1083/jcb.200511093

Hu, S., Dasbiswas, K., Guo, Z., Tee, Y.-H., Thiagarajan, V., Hersen, P., Chew, T.-L., Safran, S. A., Zaidel-Bar, R. and Bershadsky, A. D. (2017). Long-range self-organization of cytoskeletal myosin II filament stacks. *Nat. Cell Biol.* **19**, 133-141. doi:10.1038/ncb3466

Hundt, N., Steffen, W., Pathan-Chhatbar, S., Taft, M. H. and Manstein, D. J. (2016). Load-dependent modulation of non-muscle myosin-2A function by tropomyosin 4.2. *Sci. Rep.* **6**, 20554. doi:10.1038/srep20554

Masedunskas, A., Appaduray, M. A., Lucas, C. A., Lastra Cagigas, M., Heydecker, M., Holliday, M., Meiring, J. C. M., Hook, J., Kee, A., White, M. et al. (2018). Parallel assembly of actin and tropomyosin, but not myosin II, during de novo actin filament formation in live mice. *J. Cell Sci.* **131**, jcs212654. doi:10.1242/jcs.212654

Meiring, J. C. M., Bryce, N. S., Wang, Y., Taft, M. H., Manstein, D. J., Liu Lau, S., Stear, J., Hardeman, E. C. and Gunning, P. W. (2018). Co-polymers of actin and tropomyosin account for a major fraction of the human actin cytoskeleton. *Curr. Biol.* **28**, 2331-2337.e5. doi:10.1016/j.cub.2018.05.053

Pathan-Chhatbar, S., Taft, M. H., Reindl, T., Hundt, N., Latham, S. L. and Manstein, D. J. (2018). Three mammalian tropomyosin isoforms have different regulatory effects on nonmuscle myosin-2B and filamentous beta-actin in vitro. *J. Biol. Chem.* **293**, 863-875. doi:10.1074/jbc.M117.806521

Pellegrin, S. and Mellor, H. (2007). Actin stress fibres. *J. Cell Sci.* **120**, 3491-3499. doi:10.1242/jcs.018473

Percival, J. M., Hughes, J. A. I., Brown, D. L., Schevzov, G., Heimann, K., Vrhovski, B., Bryce, N., Stow, J. L. and Gunning, P. W. (2004). Targeting of a tropomyosin isoform to short microfilaments associated with the Golgi complex. *Mol. Biol. Cell* **15**, 268-280. doi:10.1091/mbc.e03-03-0176

Prasad, G. L., Fuldner, R. A. and Cooper, H. L. (1993). Expression of transduced tropomyosin 1 cDNA suppresses neoplastic growth of cells transformed by the ras oncogene. *Proc. Natl. Acad. Sci. USA* **90**, 7039-7043. doi:10.1073/pnas.90.15.7039

Sao, K., Jones, T. M., Doyle, A. D., Maity, D., Schevzov, G., Chen, Y., Gunning, P. W. and Petrie, R. J. (2019). Myosin II governs intracellular pressure and traction by distinct tropomyosin-dependent mechanisms. *Mol. Biol. Cell* **30**, 1170-1181. doi:10.1091/mbc.E18-06-0355

Schevzov, G., Vrhovski, B., Bryce, N. S., Elmir, S., Qiu, M. R., O'Neill, G. M., Yang, N., Verrills, N. M., Kavallaris, M. and Gunning, P. W. (2005). Tissue-specific tropomyosin isoform composition. *J. Histochem. Cytochem.* **53**, 557-570. doi:10.1369/jhc.4A6505.2005

Schevzov, G., Whittaker, S. P., Fath, T., Lin, J. J.-C. and Gunning, P. W. (2011). Tropomyosin isoforms and reagents. *Bioarchitecture* **1**, 135-164. doi:10.4161/bioa.1.4.17897

Tojkander, S., Gateva, G., Schevzov, G., Hotulainen, P., Naumanen, P., Martin, C., Gunning, P. W. and Lappalainen, P. (2011). A molecular pathway for myosin II recruitment to stress fibers. *Curr. Biol.* **21**, 539-550. doi:10.1016/j.cub.2011.03.007

Tojkander, S., Gateva, G. and Lappalainen, P. (2012). Actin stress fibers–assembly, dynamics and biological roles. *J. Cell Sci.* **125**, 1855-1864. doi:10.1242/jcs.098087

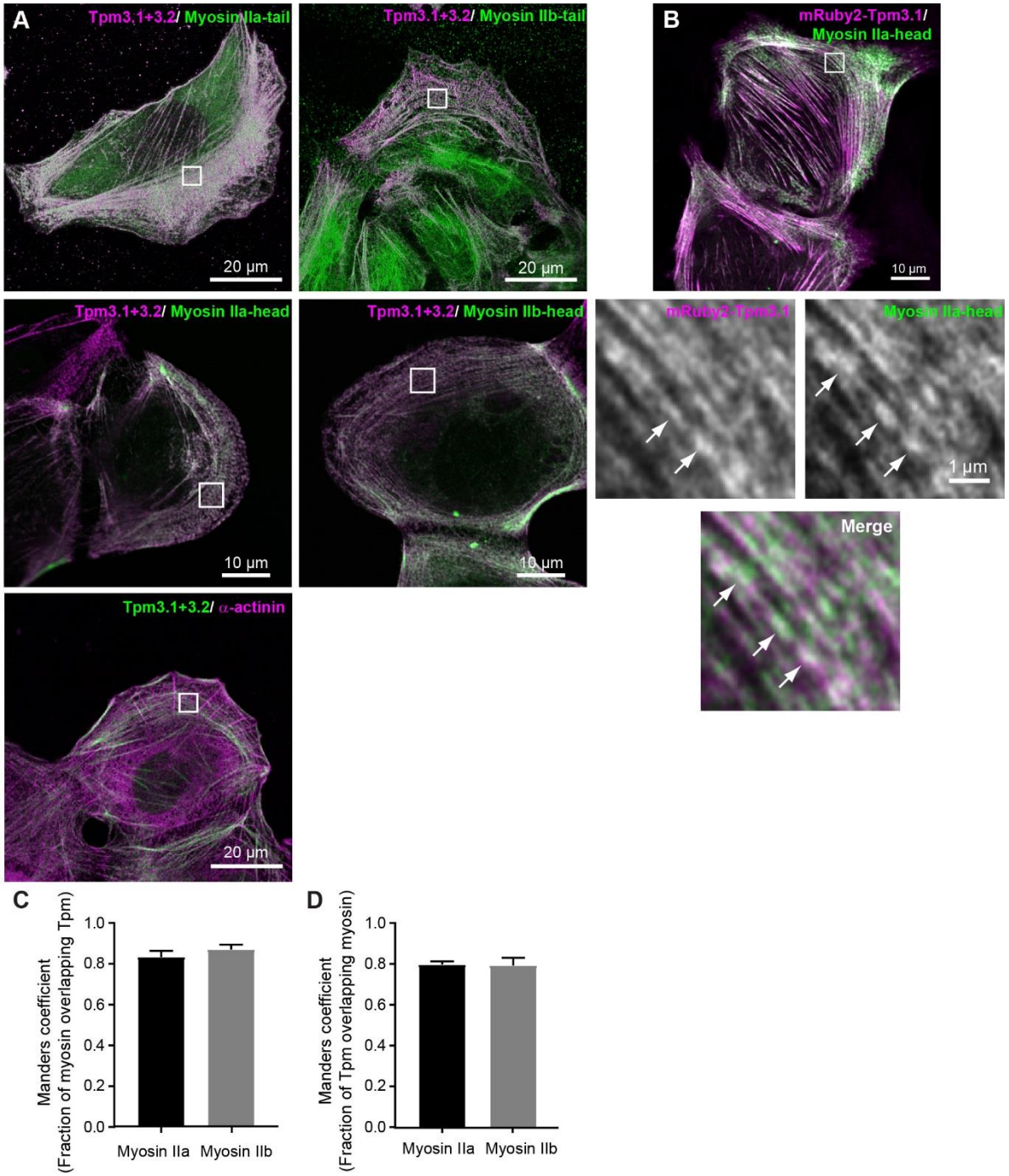

Figure S1. Tpm3.1/3.2 and Tpm4.2 co-localise with non-muscle II heads, but not non-muscle myosin II tails or α-actinin. (A) Confocal images of U2OS cells that were imaged in higher resolution in Figure 2. White boxes indicate the region imaged by STED or airyscan in Figure 2. (B) Live cell airyscan image of U2OS cells co-transfected with Ruby2-N-Tpm3.1 and myosin IIa-mEmerald demonstrate that the two constructs co-localise together at repetitive striations (arrows) along stress fibres. (C, D) Airyscan images from 3 independent experiments with 6-10 images per group per experiment were analysed for co-localisation between Tpm3.1/3.2 and Tpm4.2 with myosin IIa-mEmerald and myosin IIb-mEmerald. Graphs show mean ± SD of (C) fraction of myosin overlapping tropomyosin and (D) fraction of tropomyosin overlapping myosin.

Movie 1. Tpm3.1-APEX2 decorated actin filaments show a striated organization of Tpm3.1/3.2 in stress fibres. Tomogram reconstruction showing the 3D organization of Tpm3.1/3.2 coated actin filaments within a cultured homozygous Tpm3.1-APEX2 +/+ primary MEF. Dark enrichments correspond with Tpm3.1-APEX2 enriched regions (tomogram depth = 200 nm). Scale bar = 200 nm.

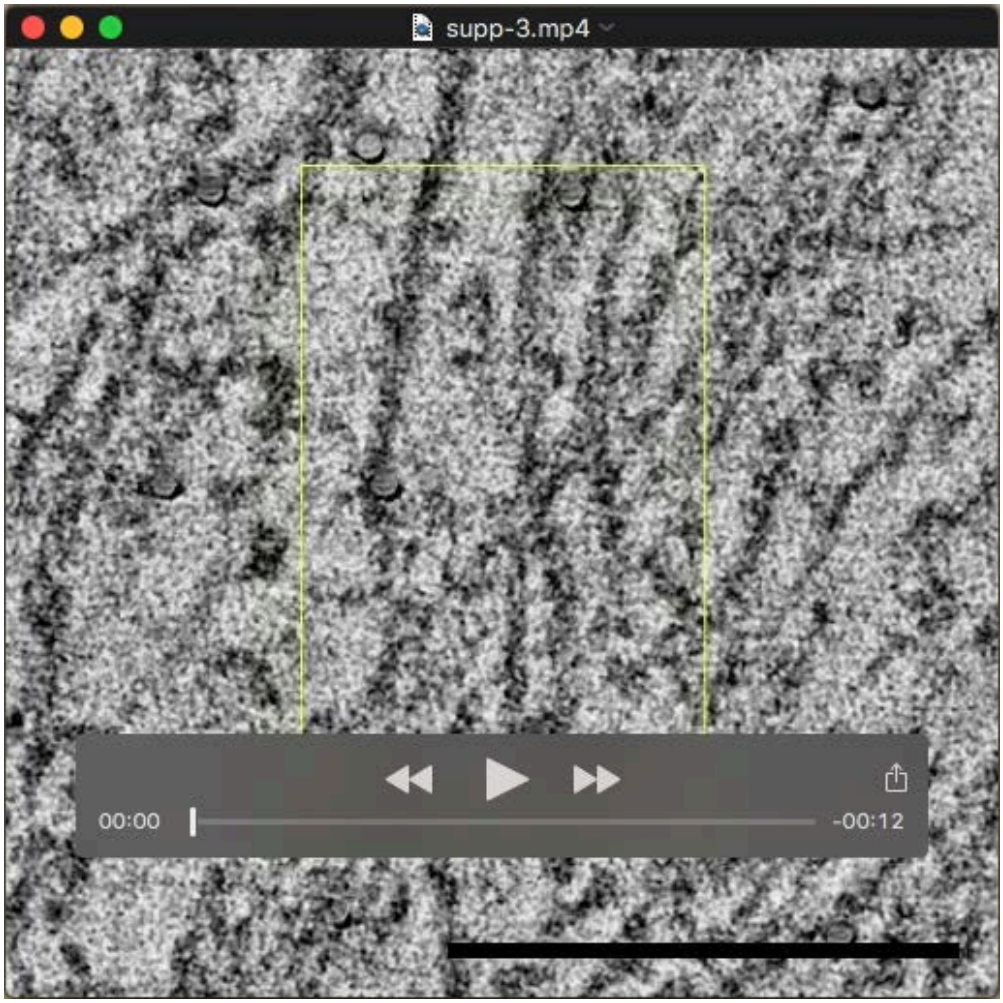

Movie 2. Tpm3.1/3.2 coated actin filaments are intact in sections processed for electron microscopy. A movie of showing a tomogram of Tpm3.1/3.2 coated actin filaments within a cultured homozygous Tpm3.1-APEX2 +/+ primary MEF. Dark enrichments correspond with APEX2-Tpm3.1 enriched regions (tomogram depth = 200 nm). Zoom-in isosurface rendering of the selected volume (magenta) highlights the intactness of the actin filaments. Scale bar = 200 nm.